Received: 5 July 2022 | Revised: 8 September 2022 | Accepted: 21 September 2022

DOI: 10.1002/mp.16006

RESEARCH ARTICLE

MEDICAL PHYSICS

Commissioning and validation of a novel commercial TPS for ocular proton therapy

Jörg Wulff[1,2,3] | **Benjamin Koska**[1,2,3] | **Jens Heufelder**[4,5] | **Martin Janson**[6] | **Claus Maximilian Bäcker**[1,2] | **Hilda Siregar**[1,2] | **Carina Behrends**[1,2,7] | **Christian Bäumer**[1,2,3,7,8] | **Andreas Foerster**[2,9] | **Nikolaos E. Bechrakis**[2,9] | **Beate Timmermann**[1,2,3,8,10]

[1]West German Proton Therapy Centre (WPE), Essen, Germany

[2]University Hospital Essen, Essen, Germany

[3]West German Cancer Centre (WTZ), Essen, Germany

[4]Department of Ophthalmology, Charité—Universitätsmedizin Berlin, Berlin, Germany

[5]Charité—Universitätsmedizin Berlin, BerlinProtonen am Helmholtz-Zentrum Berlin für Materialien und Energie, Berlin, Germany

[6]RaySearch Laboratories, Stockholm, Sweden

[7]Department of Physics, TU Dortmund University, Dortmund, Germany

[8]German Cancer Consortium (DKTK), Essen, Germany

[9]Department of Ophthalmology, University Hospital Essen, Essen, Germany

[10]Department of Particle Therapy, University Hospital Essen, Essen, Germany

Correspondence
Jörg Wulff, Westdeutsches Protonentherapiezentrum Essen (WPE) gGmbH, Am Mühlenbach 1, 45147 Essen, Germany.
Email: joerg.wulff@uk-essen.de

Abstract

Background: Until today, the majority of ocular proton treatments worldwide were planned with the EYEPLAN treatment planning system (TPS). Recently, the commercial, computed tomography (CT)-based TPS for ocular proton therapy RayOcular was released, which follows the general concepts of model-based treatment planning approach in conjunction with a pencil-beam-type dose algorithm (PBA).

Purpose: To validate RayOcular with respect to two main features: accurate geometrical representation of the eye model and accuracy of its dose calculation algorithm in combination with an Ion Beam Applications (IBA) eye treatment delivery system.

Methods: Different 3D-printed eye-ball-phantoms were fabricated to test the geometrical representation of the corresponding CT-based model, both in orthogonal 2D images for X-ray image overlay and in fundus view overlaid with a funduscopy. For the latter, the phantom was equipped with a lens matching refraction of the human eye. Funduscopy was acquired in a Zeiss Claus 500 camera. Tantalum clips and fiducials attached to the phantoms were localized in the TPS model, and residual deviations to the actual position in X-ray images for various orientations of the phantom were determined, after the nominal eye orientation was corrected in RayOcular to obtain a best overall fit. In the fundus view, deviations between known and displayed distances were measured. Dose calculation accuracy of the PBA on a 0.2 mm grid was investigated by comparing between measured lateral and depth–dose profiles in water for various combinations of range, modulation, and field-size. Ultimately, the modeling of dose distributions behind wedges was tested. A 1D gamma-test was applied, and the lateral and distal penumbra were further compared.

Results: Average residuals between model clips and visible clips/fiducials in orthogonal X-ray images were within 0.3 mm, including different orientations of the phantom. The differences between measured distances on the registered funduscopy image in the RayOcular fundus view and the known ground-truth were within 1 mm up to 10.5 mm distance from the posterior pole. No clear

Jörg Wulff and Benjamin Koska contributed equally to this work.

benefit projection of either polar mode or camera mode could be identified, the latter mimicking camera properties. Measured dose distributions were reproduced with gamma-test pass-rates of >95% with 2%/0.3 mm for depth and lateral profiles in the middle of spread-out Bragg-peaks. Distal falloff and lateral penumbra were within 0.2 mm for fields without a wedge. For shallow depths, the agreement was worse, reaching pass-rates down to 80% with 5%/0.3 mm when comparing lateral profiles in air. This is caused by low-energy protons from a scatter source in the IBA system not modeled by RayOcular. Dose distributions modified by wedges were reproduced, matching the wedge-induced broadening of the lateral penumbra to within 0.4 mm for the investigated cases and showing the excess dose within the field due to wedge scatter.

Conclusion: RayOcular was validated for its use with an IBA single scattering delivery nozzle. Geometric modeling of the eye and representation of 2D projections fulfill clinical requirements. The PBA dose calculation reproduces measured distributions and allows explicit handling of wedges, overcoming approximations of simpler dose calculation algorithms used in other systems.

KEYWORDS
proton therapy, RayOcular, uveal melanoma

1 | INTRODUCTION

Ocular proton therapy (OPT) started in the 1970s at the Massachusetts General Hospital[1] and since then more than 30 000 patients have been treated for ocular tumors worldwide with local tumor control rates at or above 95%.[2] The first available treatment planning system (TPS) was EYEPLAN, which has been steadily developed[3,4] and is still used for a majority of all OPT treatment plans worldwide.[2] EYEPLAN is, however, not a medical product and was developed by various groups.[3] Despite its proven usability over several decades, there is no life cycle management provided by a vendor, precluding it from certification as medical software. There are in fact only a few alternatives to EYEPLAN. Varian (Varian Medical Systems, Palo Alto, USA) has released a commercial OPT planning system named "Eclipse Ocular Proton Planning" (EOPP) that inherited many of its features from EYEPLAN.[5–7] The German cancer research center developed the OCTOPUS planning system[8,9] that was later brought to clinical use at the Helmholtz-Zentrum Berlin, Germany.[10] Recently, Fleury et al. reported on the in-house development of a magnetic resonance imaging (MRI)-based planning tool,[11] which has not been used clinically. RaySearch (RaySearch Laboratories, Stockholm, Sweden) released a module for the RayStation TPS named RayOcular that fulfills the existing requirements of OPT but also adds new functionalities.

All clinically used systems share a model-based approach, that is, the eye is represented by a parametrized geometric model of the human eye. The anatomy outside of the eye is simplified as a homogenous volume, limited by a "skin-plane" perpendicular to the beam-direction and at a user-defined position relative to the outer surface. Thus, structures like the lacrimal glands, lids, or bones are not considered. In EYEPLAN and EOPP, the eye model and clip positions are created by information from, for example, physical measures, ultrasonic, and X-ray images, whereas OCTOPUS and RayOcular use computed tomography (CT) and MRI images in the modeling process.[9,12] The dose calculation in EYEPLAN, EOPP, and OCTOPUS is based on simplistic lookup tables that use measured lateral and distal penumbrae to construct a three-dimensional dose distribution. This approximation is generally accepted, but dose deviations become more relevant, especially when wedges are applied.[13,14] As a result, the planning is driven by the experience of the planner, intrinsically taking the limitations in accuracy into account, for example, by increased margins or manually increasing the field opening behind the wedge. In RayOcular, on the other hand, dose calculation is based on a pencil-beam algorithm (PBA), which is expected to be more accurate than the lookup algorithms, especially when the proton beam passes a wedge and air gap before entering the patient.

In EYEPLAN and EOPP, the target structure is defined in a fundus view, which mimics the view of a fundus camera. In later versions of EYEPLAN, it is possible to register a funduscopic image in the fundus view to improve the definition of the tumor-based contour.[4] OCTOPUS and RayOcular also support target definition in fundus view with registered funduscopy images. However, what these two systems add is the possibility to define the target volume from MRI volumetric images. This has been shown to significantly improve the tumor volume definition for large and/or anterior positioned tumors allowing for a reduction by a factor of up to 2.2 without compromising safety.[15]

The funduscopy image can be considered an important source of information about the tumor and guides the delineation of the target in OPT.[2–4] However, uncertainties in the funduscopic imaging, the registration to the model, and the projection of the eye model into the fundus view may have an impact on the accuracy of the planning target volume. The overall uncertainty is generally taken into account during the planning by utilizing additional planning margins. It is understood that a possible camera distortion increases with distance from the anterior pole, and Daftari et al. estimated the impact to be up to 2.5 mm.[4] To the authors' knowledge, a rigorous test with a known ground truth has not been conducted to quantify the accuracy of fundus overlay in OPT planning.

The West German Proton Therapy Centre Essen (WPE) started a clinical treatment of uveal melanoma in late 2021, based on treatment plans created in RayOcular. RayOcular was employed in a previous in silico study to investigate the impact of lateral and distal penumbra on dose distributions in uveal melanoma cases.[12] Prior to clinical first use, the system in version RayStation 10B was validated with the dedicated eye nozzle of the ProteusPlus proton beam delivery system of IBA (Ion Beam Applications, Louvain-la-Neuve, Belgium).[16] The current manuscript summarizes two fundamental aspects of this validation. First, the geometric modeling of the eye with projection into 2D images for overlay with X-ray and funduscopy images was investigated with developed phantoms. Second, the measurement-based validation focused on the accuracy of calculated dose distributions, including the use of wedges.

2 | MATERIALS AND METHODS

2.1 | General functionalities of the RayOcular TPS

RayOcular is a module within the RayStation TPS and thus shares many of the standard RayStation functionalities, such as patient-data handling, image registration, contouring, display and evaluation of dose metrics. The general approach follows the ideas of EYEPLAN: The eye is approximated using a set of structures such as the sclera, retina, and lens parametrizing a model of the patient's eye that is organized hierarchically. Dependencies between the components allow for structures to be modified through resizing of single structures (e.g., changing the dimensions of the sclera will change dimensions of the other structures).

The model is built upon volumetric CT images, which typically allow determining the outer sclera, lens, and optical nerve. The adjustments of size and location of those structures are possible and may further be guided by the information visible in a registered MRI. The eye model can also be fully defined from external measures such as axial length, limbus diameter, or cornea-lens distance, as is commonly done in EYEPLAN. In contrary, each component of the model may be modified or new structures may be defined by contouring in volumetric CT/MRI image sets with the standard contouring tools of RayStation. Clip locations (center of gravity) are identified in the CT/MR image views and constructed as 3D models with 2.5 mm diameter and 0.3 mm thickness, tangential to the model sclera. The clips can subsequently be verified by projecting them onto imported orthogonal X-ray image pairs for a given (nominal) orientation of the eye, which is the eye center position and the eye gaze as given by the fixation light's polar and azimuthal angles. Subsequently apparent values can be defined, also including the eye twist angle, to provide a best fit of the modeled clips to the clips appearing in the X-ray images. Note, the direct definition of the clip positions from the X-rays is not yet supported in RayOcular. Once the eye model is constructed, various metrics are displayed to the user, including the clip-to-clip, clip-to-limbus, and clip-to-sclera distances. Examples of eye models generated within RayOcular can be found in Ref. [12].

RayOcular includes a fundus view that supports two modes of projection: polar and camera mode. In polar mode, the 3D eye model is projected into a 2D plane following the description of Dobler et al.,[9] which is similar to the approach used in EYEPLAN. The camera mode tries to mimic the properties of the used fundus camera and has several adjustable parameters, such as image size, field of view, and an optics fit-factor. The curved plane that is projected in the fundus view can be continuously chosen from the inner plane of the retina (the plane seen by the fundus camera) to the outer plane of the sclera (where the clips are attached). Besides the outlines of the eye model and target components, the fundus view in RayOcular can also show CT/MR image data and dose at the chosen plane. It is further possible to register a funduscopy image by scaling, translation, and rotation of imported 2D images. The fundus view includes a measure tool that gives the Euclidean distances in the 3D model between two points defined in the fundus view.

Following the concepts of EYEPLAN, target structures can be created in the fundus view by defining the base contour. The convex extension into the eyeball is then constructed from a polynomial function with a user-provided apex location and height. The target contour can further be modified, or completely be derived from contouring in volumetric CT/MRI image sets—an approach also useful for contouring of iris or conjunctival melanoma, for which no funduscopy is available. Note, handling of anterior photographs is currently not implemented in RayOcular. The volume of a fundus view defined target is included in the 2D CT/MR image, and the base contour of a target volume defined by regular contouring can be seen in the fundus view.

The dose calculation in RayOcular is based on the existing PBA[17] available in RayStation for, for example,

double scattering and uniform scanning delivery techniques.[7] The major new features are a selectable dose grid resolution down to 0.2 mm and the possibility to include an aperture mounted wedge. In brief, the PBA employs a discretized energy spectrum of protons as determined during commissioning, one for each range modulator wheel, that is, each spread-out Bragg peak (SOBP). The energy spectrum is only valid within a specific interval in prescribed range (R) that follows the corresponding intervals of the IBA delivery system, there referred to as "Options" as further elucidated in Section 2.3.1 and realized by range-modulator wheels. Change of range for an SOBP within an Option in the software is achieved by a water-equivalent shift of the energy layer–integrated depth–doses (IDDs), effectively reducing the range of the complete modeled curve. In the dose calculation, the spectrum is subdivided into "energy layers" that are separately traced in the PB dose engine. The IDD used for each layer in the dose calculation is determined by a superposition of pre-calculated mono-energetic IDDs according to the sub-energy spectrum of the layer. It should be noted that these energy layers generally will not coincide with the energy layers generated by the range modulator wheel. The lateral spatial–angular distribution is described by a point source with defined position and angular spread. The same effective point source is used for all energy layers, irrespective of the thickness of range modulation material for that layer. The lateral fluence distribution of protons upstream of the aperture is assumed to be flat. The lateral spread in medium considers multiple Coulomb scattering with Rossi scattering power as well as nuclear scattering based on a modified version of Soukup et al.[18] The latter is optional and was turned off for the calculations presented in this study as the nuclear halo effect for the shallow fields is limited but extends the dose calculation times. Different materials can be assigned to the different eye model components, and the material composition is considered in the PBA. The energy loss and scattering in a wedge is calculated with the same approach.

The commissioning of RayStation is performed by RaySearch based on users' provided measurements. In brief, an Error-function expression[19] is fitted to the lateral profile of a squared field at a depth corresponding to the middle of the SOBP. With known size and position of the aperture used, the width of this fit yields the virtual source–axis distance (SAD), and its standard deviation in air angular variance of the protons, after the subtraction of the beam spread in the water-phantom. One lateral field is typically measured per option. The depth profile for each option and modulation is used to find an energy spectrum for the entire SOBP, which in the dose calculation is divided into energy layer spectra represented in steps of 1 cm in water.

2.2 | Validation of eye modeling

2.2.1 | Projection of clip positions in planar X-ray imaging

Two phantoms were created to test the capabilities of RayOcular. The first was a simple ball with standard Tantalum clips that are used clinically (diameter 2.5 mm and height 0.25 mm) glued to its surface (Figure 1a). This phantom served to test the clips' geometric representation in the overlay to X-rays, but without the possibility to precisely define the orientation of the phantom. The physical clip-to-clip distances were measured with a caliper and compared to the metrics provided in RayOcular.

The second phantom (Figure 1b) was 3D printed with a Form2 printer (Formlabs, MA, USA) facilitating various well-defined orientations in terms of polar and azimuth gaze angles. The phantom was designed with an indexing scheme allowing for discrete angles in 10°–15° steps. Instead of Tantalum clips, radiopaque spherical fiducials with 1.5 mm diameter-type "Beekley X-SPOT" (Beekley Medical, Bristol, USA) were embedded in the phantom. These fiducials exhibit much smaller CT reconstruction artifacts as compared to Tantalum. The phantom was positioned with its rotational center aligned with the isocenter of the delivery system; thus, in the evaluation, the gaze angles and the fixation light angles are identical.

In both cases, the phantom was scanned with a Philips Big Bore Brilliance CT scanner (Philips Medical Systems, Best, the Netherlands) employing a dedicated ORBITA protocol (120 kV, 0.6 mm slices, reconstruction with 0.1 mm pixel size) and a corresponding eye model was created in RayOcular. The outer dimensions of the sclera model structure were adjusted to fit the visible surface of the phantom. The clip locations were identified as the center of gravity in the Tantalum clip reconstruction artifacts (ball-phantom) and fiducials (3D-printed phantom). RayOcular automatically fits the clip orientations to be tangential to the 3D surface of the outer sclera. Orthogonal X-ray images of the phantom were acquired and imported to RayStation in the RayOcular setup workspace. The imaging system of the IBA eye treatment room was previously defined in RayStation in terms of SAD, source-to-imager distance (SID), imager size, and "gantry" angles with respect to the beam coordinate system.

The ball-phantom (Figure 1a) was imaged in several approximate orientations to validate the correct representation of the clips in various orientations. The best agreement between the clips in the two X-ray images and modeled clips was then determined by adjusting the apparent eye center position, fixation light position, and eye twist rotation in the RayOcular setup workspace. The residual deviation was determined in the overlay of

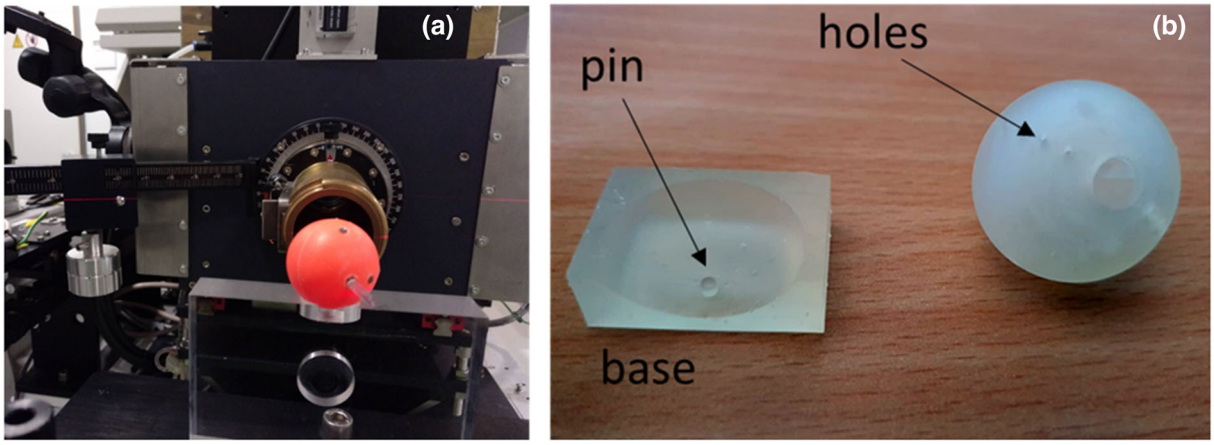

FIGURE 1 (a) Ball-phantom with glued Tantalum clips on its surface placed at isocenter in front of the Ion Beam Applications (IBA) system snout. (b) 3D-printed phantom (right) with its base-plate (left) allowing for realizing a polar/azimuthal gaze angle in discrete steps. The phantom has holes in 10°–15° steps fitting to the pin of the base-plate.

both imaging directions as follows. The deviation was calculated as Euclidean distance for each clip, using the average distance for same directions in the Cartesian coordinate system of both views. Finally, the average of all four clips was taken as the remaining residual.

The 3D-printed phantom (Figure 1b), on the other hand, was aligned by the room lasers in 24 gaze angle orientations using the aforementioned indexing. The orientation of the eye model was then again fine-tuned in RayOcular by adjusting the apparent eye center, fixation light position, and twist. For each orientation, the residuals were calculated as outlined before.

2.2.2 | Representation in funduscopy imaging

The funduscopy image can be considered an important source of information about the tumor and guides the delineation of the target in OPT.[2–4] Any uncertainty in the funduscopic image, the registration to the model, and the projection of the eye model into the fundus view may have an impact on the accuracy of the planning target volume. This uncertainty is generally taken into account during the planning. It is understood that a possible distortion increases with distance from the anterior pole. Daftari et al. estimated the impact to be up to 2.5 mm.[4]

Apart from possible distortions of the actual funduscopy, the projection of the 3D eye model into the fundus view in RayOcular needs to be correct.

To validate the accuracy of the fundus view and funduscopic image registration in RayOcular, a phantom was constructed, consisting of a 3D-printed hollow sphere with red filament, filled with distilled water, and closed by a lens (Kaps Vision GmbH, Rathenow, Germany) (see Figure 2, "Fundus phantom"). The refraction power of the selected lens was 60 diopters (dp), which is close to a human eye that shows 59–71 dp. The refraction index of the lens material CR39 is 1.498, whereas the human eye lens has a slightly lower refraction index ranging between 1.37 and 1.42.[20] The phantom was matched in size to a human eye (diameter 23 mm) and includes landmarks consisting of holes distributed horizontally and vertically from the posterior pole at a 2 mm distance (10° separation as seen from the eye center). To mimic the clips of an eye patient, four additional holes at different positions (see Figure 2) were included in which fiducials were glued (Beekley X-SPOT). A CT image of the phantom was subsequently taken and imported to RayOcular in which an eye model, including clips, was constructed.

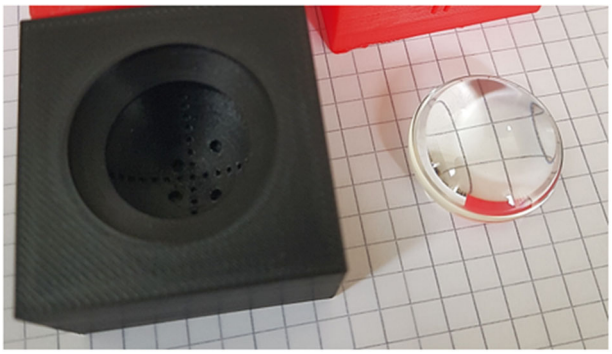

FIGURE 2 3D-printed eye-phantom for testing the fundus camera with artificial lens ("Fundus phantom"). The inner surface is equipped with observable landmarks, which are single holes along the main axes in 10° steps. Four holes further allow to embed fiducials. Note, a version printed with red filament was used for imaging.

A funduscopy image (single wide-field, resolution 7.3 μm/pixel) of the phantom was acquired with a Zeiss CLARUS 500 (Carl Zeiss Meditec, Dublin, USA) and images exported in *jpg-format. The funduscopy image was imported to RayOcular and manually registered to the fundus view. The registration was achieved by

matching the size of the posterior hole of the phantom that has a known diameter of 1 mm. This is similar to the clinical practice where the visible distance between macula and optical disc is used to scale the image to the model, based upon measurements in optical coherence tomography (OCT). Rotations and translations were manually set to match the visible landmarks in the phantom. The field-of-view angle in the RayOcular camera mode settings was deduced from the specification of the CLARUS 500 with 133°, whereas the other camera mode optical parameters were based on a best guess (focal point on cornea, correction for optical refraction = 0, film size = 5 cm).

The distances from posterior pole to the different horizontal and vertical landmarks seen in the registered image, as well as the landmark-to-landmark distances were measured in the RayOcular fundus view (resolution 0.1 mm) and compared to the known values of the phantom. Landmarks up to 60° away from the posterior pole were included, corresponding to 11.5 mm Euclidean distance.

2.3 | Dosimetric validation

2.3.1 | The IBA delivery system at WPE

The basic design of the IBA eye treatment system is described in Slopsema et al.,[16] with the difference that the WPE system is commissioned with 82.5 MeV initial energy rather than 105 MeV as in Ref. [16]. Briefly the design consists of the proton beam hitting Tantalum and/or Lucite scatter foils behind a spinning range-modulator wheel. Each exchangeable wheel creates a "full-plateau" SOBP, that is, a flat dose level up to the surface. The wheel can be equipped with so-called stop-blocks made of brass, which define the proximal extent of the SOBP. Each of the seven wheels (Options) in the WPE system is designed to give a flat SOBP within a given interval in distal range (R) interval ranging from 35 down to 5 mm, defined by the $R90$ depth. Within each interval, the flatness of the SOBP is well within 2.0%. The stopblocks allow for modulation (M) steps of ~1 mm on average (<2.7 mm maximum step width), leading to a total of 145 wheel/stop-block combinations (also referred to as "Sub-Options"). Modulation is defined by the distance between the proximal and distal 95% level. The isocenter of the IBA system is located 70 mm behind the downstream aperture surface.

The IBA system at WPE comes with three poly(methyl methacrylate) (PMMA) wedges of different physical angles, that is, 26.3°, 40.5°, and 56°. The wedges are attached to patient-specific aperture by two pins, allowing for a rotation of the wedge as well as a variable lateral position of the thin edge from beam center, with an estimated positional uncertainty of 0.1 mm due to the manufacturing process.

The imaging system consists of a pair of orthogonal X-ray sources and detectors with (AP/LAT) and (AP/LAT) SIDs of 192 and 182 cm, respectively. Each image detector is equipped with a cross-wire that is aligned with the system isocenter and creates a visible shadow in the image.

2.3.2 | Beam data used for beam modeling

The commissioning of the beam-model was performed by RaySearch, based on a set of measured depth–doses and lateral profiles in water (see Section 2.1). All measured data was obtained without wedges, as RayOcular does not require any additional beam data for the wedge models, only the physical properties such as wedge angle and material are included in the beam model.

Depth–dose profiles along the central axis were acquired with an Advanced Markus (type 34045) plane-parallel ionization chamber in a modified PTW MP3-XS water tank (PTW-Freiburg, Freiburg, Germany). As the original tank wall is made of 2 cm PMMA, a hole was drilled into the wall and a thin entrance window made of PMMA was tightly screwed to the wall. The water-equivalent thickness (WET) of the window used was determined to be 1.16 mm by distal profile measurements with and without the window in front of the phantom equipped with another window. In all measurements a 20 mm × 20 mm aperture was used and the phantom surface placed at isocenter, that is, 7 cm away from the downstream aperture surface. Prior to the acquisition of the curve, the chamber was centered laterally. The uncertainty of absolute water-equivalent depth assigned to each measurement point was estimated to be 0.15 mm, taking the definition of zero-position, WET of chamber, and entrance window as well as linear motor precision into account. The step-size for the acquisition of the depth–dose profiles was 0.2 mm in the distal falloff (DFO) and 0.3 mm elsewhere. One depth–dose profile for each available wheel/stop-block combination at a range corresponding to the maximum range of the wheel was recorded.

Lateral profiles were acquired at the middle depth of each wheel with maximum modulation with the chamber at isocenter, that is, the phantom was shifted for each measurement. A PTW microSilicon diode detector (type 60023) was employed for all scans in axial orientation. The diode was chosen as it has a small volume and showed no LET dependence in SOBP scans. The detector has a sensitive volume with radius of 0.75 mm and thickness of 18 μm. The WET of the housing was taken from the product sheet and considered in the definition of measurement depth. Prior to each measurement series, a lateral scan was taken for the alignment of the detector with the aperture center. This procedure

also allowed for a pre-irradiation with ~10–15 Gy. The uncertainty of the lateral placement was estimated with 0.2 mm, taking the procedure of centering and the precision of the water tank motors into account. The step-size for lateral in- and cross-line profiles scans was 0.2 mm in the penumbra region and 0.3 mm elsewhere. Profiles were acquired with the detector at isocenter plane in the middle of the full-plateau SOBP. Hence, the position of the water-phantom surface was different in each wheel. The field was collimated by a 20 mm × 20 mm and 10 mm × 10 mm aperture.

In total, 152 depth and 28 lateral profiles were acquired.

2.3.3 | Beam data for evaluation

Besides the depth–dose and lateral profiles acquired for the commissioning (Section 2.3.2), more profiles were acquired, including lateral profiles at other depths and free in air for some wheel/stop-block combinations. Lateral profiles were acquired as described in Section 2.3.2 for various circular apertures with diameters of 3, 5, 10, 15, 20, and 30 mm. These measurements were performed with the phantom surface at isocenter and a field with $R = 25$ mm, $M = 20$ mm ($R25M20$). The fields with circular opening were also used to determine the output-factor relative to a 20 mm × 20 mm field in the middle of the SOBP for $R25M20$ and $R10M11$.

Additionally, dose was measured behind three wedges and compared to the calculations. Lateral as well as depth–dose curves were measured for the three available wedges (see Section 2.3.1) with the microSilicon detector. Depth–dose curves were measured behind the wedge in the center of a 20 mm × 20 mm aperture, with the thin edge of the wedge shifted by −5 mm, that is, the wedge was covering the central axis. Lateral profiles were taken in two depths d: $d = R - 2/3M$ and $d = R - M/3$. Three different range and modulation combinations were tested, that is, $R10M10$, $R25M25$, $R35M35$, to cover expected extreme wheel/stop-block combinations utilizing a wedge. The phantom surface was positioned at isocenter for all measurements. The dose calculations with wedges were based on an evaluation version of RayOcular 10B as support for proton wedges was not yet clinically released at the time of the study (expected in RayStation 12A release).

All measured profiles were compared to the calculations of the TPS in terms of a 1D gamma-test implemented in GNU Octave (version 5.2),[21,22] using a threshold dose of 5% and with global normalization. The measured profiles were normalized to the center of the profiles. Lateral profiles were further centered prior to analysis, using the center between the 50% points of the normalized profile. All calculations in RayOcular were performed on an isotropic dose grid with 0.2 mm resolution.

The PBA in RayOcular does not calculate the monitor units (MUs) for a prescribed dose. Hence, each treatment field (wheel/stop-block combination) needs to be calibrated by other means, for example, by an MU model as described by Slopsema et al.[16] The comparisons in this work were all made on relative dose distributions, except for the output-factor comparisons where a constant number of MU was applied for each aperture diameter.

2.3.4 | Evaluation passing criteria

The clinical requirements for OPT are not clearly defined in literature. A 2% dose threshold was motivated by AAPM TG 157,[23] where a 2%/2 mm is recommended for relative profiles. Note, that AAPM TG 157 does not provide further information about thresholds, normalization, and acceptable pass-rates. The 2 mm distance-to-agreement (DTA) criterion is considered too large for ocular treatment, where tighter margins for the model agreement are expected.[12] The DTA of 0.3 mm was considered appropriate and is in-line with the RayOcular reference manual, stating validation criteria of 95% passing a gamma-test with 3%/0.3 mm and 98% with 5%/0.5 mm and an agreement of lateral/distal penumbra (80/20%) within 0.3 mm.[17] A determination of range for one of the wheel/stop-block combinations in the IBA system at WPE reveals a slight drift of ±0.3 mm over a period of 6 months. The derived quality assurance procedure at WPE for individual patient plans considers a 0.5 mm DTA threshold.

3 | RESULTS

3.1 | Validation of eye modeling

3.1.1 | Representation of the eye model in X-ray images

Figure 3 shows an example of matching the model clips to the X-ray images of the ball-phantom in Figure 1a within the RayOcular setup workspace. The determined residuals for all clips were on average 0.25 mm with the single clips showing a deviation of up to 0.3 mm. The remaining deviation includes the uncertainty of the manual search for best apparent eye position and angles, but also the localization of model clips within the CT of the phantom. The Tantalum clips exhibit severe reconstruction artifacts (Figure 3b) whose centers of gravity are expected to represent the clips' centers. The agreement of clip-to-clip distances measured with a caliper and calculated by RayOcular based on the localization in the CT ranged between 0.1 and 0.3 mm.

The 24 X-ray images for different orientations of the 3D-printed phantom shown in Figure 1b were used for

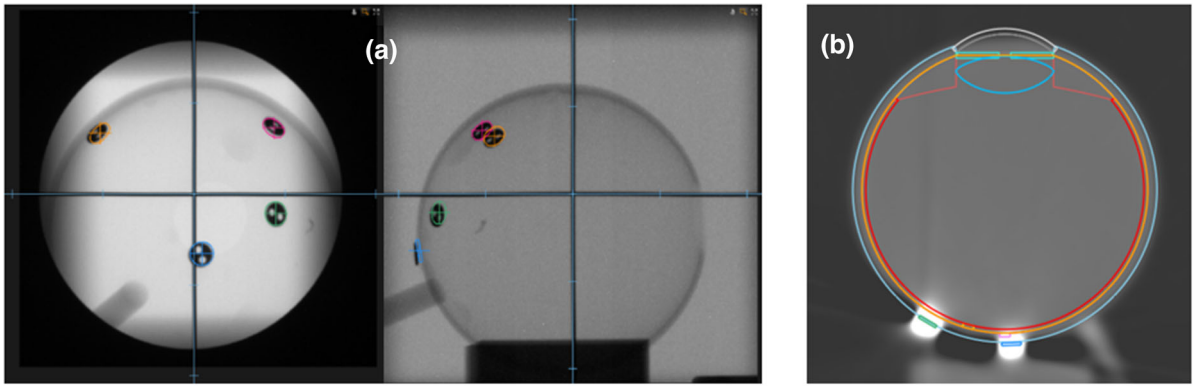

FIGURE 3 (a) Orthogonal X-ray image pair of ball-phantom in Figure 1a after matching the model clips. The colored circles are the model clips as resulting from a localization within the computed tomography (CT) of the ball-phantom. The blue cross-hair indicates the imaging isocenter per image. (b) CT of the phantom showing the model structures as well as the clip artifacts at the lower bottom.

TABLE 1 Residual deviation between the four fiducial centers and model clips for different nominal gaze angles of phantom in Figure 1b, determined in the two X-ray images

Gaze angle		Marker position residuals/mm		
Polar/°	Azimuthal/°	Average	Min	Max
30	0	0.25	0.21	0.33
30	270	0.31	0.25	0.38
24.8	141.9	0.31	0.23	0.40
41.4	135	0.29	0.15	0.36
24.8	321.9	0.25	0.18	0.38
45.9	100.2	0.24	0.15	0.35
40	0	0.21	0.10	0.40
45	90	0.23	0.10	0.50

the clip matching in RayOcular. The matching procedure included adjustments of the polar/azimuthal and twist angles from the calculated angles achieved with the indexing. The difference between nominal and apparent gaze angles was below 1° on average and never larger than 3°. The resulting mean residual deviation of the four fiducials for all 24 orientations was 0.26 mm with a maximum deviation of 0.5 mm for a single clip. Table 1 summarizes the results.

3.1.2 | Handling of funduscopy images

Figure 4a shows the registered funduscopy image of the Fundus phantom (Figure 2) in the RayOcular fundus view. Figure 4b summarizes the deviations between measured and fundus view obtained distances between the horizontal and vertical landmarks on the inner surface of the phantom and the posterior pole. The deviation is depicted as a function of angle between the posterior pole and the center of the observed hole. A maximum deviation of ~0.8 mm occurred for one of the landmarks, whereas the average was <0.2 mm.

Figure 4b also shows that the deviation is very similar for the two projection types: polar and camera. A linear fit to the deviations determined show a dependence on the distance from posterior pole, that is, toward the anterior regions in the fundus view. For both projection modes, the landmark-to-landmark distances deviated by not more than 0.1 mm from the nominal value of 2 mm as printed in the phantom surface.

3.2 | Dosimetric validation

3.2.1 | Depth–dose curves and lateral profiles

All of the 152 depth–dose curves that were used in the beam modeling showed a pass-rate of 100% for a gamma-test with 1%/0.3 mm. The range agreed within 0.1 mm, and the distal penumbra between 90% and 10% matched within less than 0.1 mm. Figure 5a shows the measured and calculated depth–dose curves for six setups at beam modeling conditions with nominal ranges R from 1.0 to 3.2 cm. Noticeably, the dose inflections in the distal part of the SOBP are well reproduced by the PBA. Figure 5b shows examples of SOBPs with different modulations within a single range-modulator wheel (#2), with a range span of 2.4–2.7 cm. The SOBP for the lowest range in this wheel is shown, and a small difference in the slope of the SOBP plateau can be observed. This is explained by the fact that the PBA in RayOcular considers the lower range by a WET shift of the curve at maximum range. However, given the rather limited available range intervals per wheel in the IBA system, the omission of slope change leads to local deviations <1%, and thus the gamma-pass-rate is still 100% for all measured curves.

All 28 in- and cross-line lateral profiles for the 20 × 20 mm^2 and a 10 × 10 mm^2 apertures that were used in the beam modeling were calculated in RayOcular with gamma-pass-rates >90% (1%/0.3 mm),

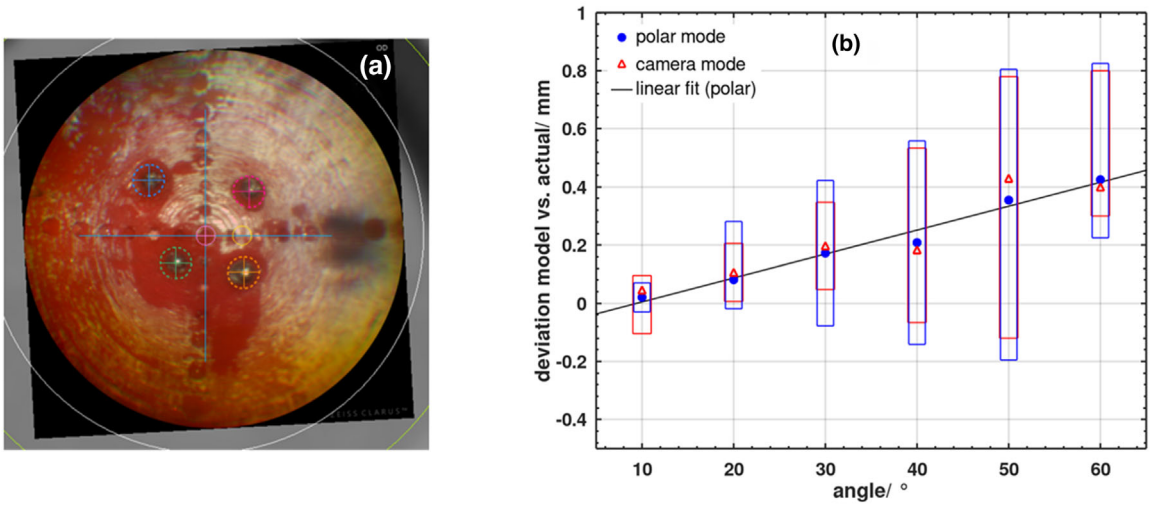

FIGURE 4 (a) Funduscopy image of the eye-phantom shown in Figure 2 as registered in the RayOcular fundus view (polar mode). The model clips are overlaid to the visible Beekley spots. (b) Deviation of the distance between the posterior pole and landmarks obtained from the RayOcular fundus view and as measured in the phantom, plotted as a function of the eye center angle between posterior pole and landmark. The deviations are shown with the image registered to the fundus view in both polar and camera modes as s mean value of the four directions (symbols). The boxes represent the minimum and maximum deviations. The solid line shows a linear fit for the polar mode measurements. The angle of 60° corresponds to a Euclidean distance of 11.5 mm.

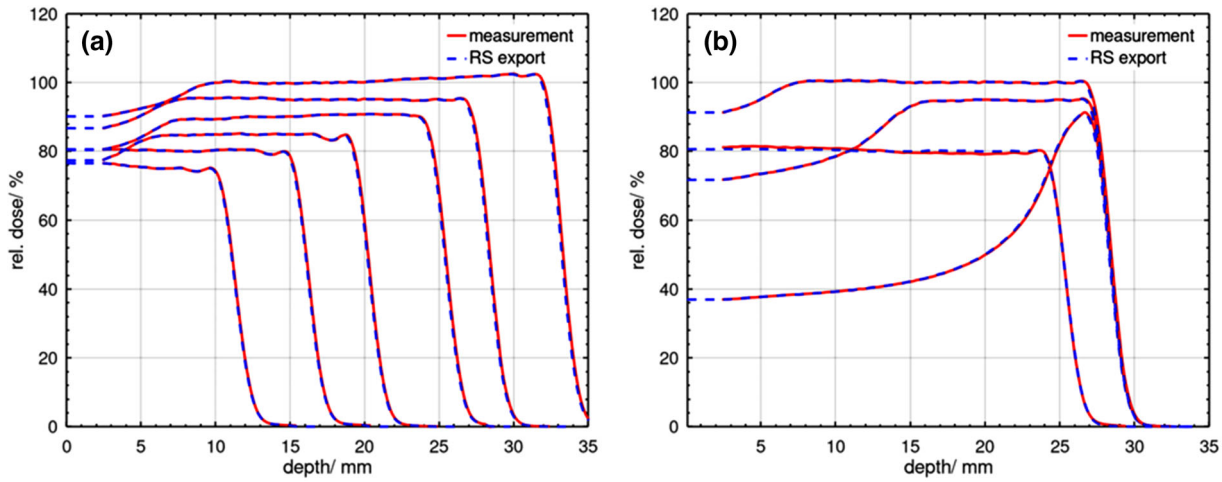

FIGURE 5 Comparison between measured and modeled depth–dose curves for (a) setups at maximum range in six range-modulator wheels and (b) for different modulations and distal ranges of the same wheel. An aperture of 20 × 20 mm was used for all fields. All dose curves are normalized to respective spread-out Bragg peak (SOBP) center. (Profiles are scaled vertically to avoid overlap in the plot.)

>98% (2%/0.3 mm), and 100% (3%/0.3 mm). The lateral penumbra (80%–20%) were reproduced within <0.1 mm for all profiles. Measurements and calculations were taken at the depth of the SOBP center for all seven range-modulator wheels with the detector placed at isocenter.

Figure 6a shows a comparison of the *R*25*M*20 mid SOBP cross-profiles with circular apertures of 3, 5, 10, 15, 20, and 30 mm in diameter. The isocenter was placed at phantom surface, thus differing from the commissioning setup. Again, pass-rates >90% (1%/0.3 mm), >98% (2%/0.3 mm), and 100% (3%/0.3 mm) were achieved and the difference in the lateral penumbra was within 0.1–0.2 mm, varying with field-size (see Table A1).

Figure 6b shows lateral cross-profiles of the *R*25*M*20 field with a 20 mm × 20 mm aperture, in air and at various depths in water. The measured in air and shallow depth profiles exhibit slightly domed shapes that are not reproduced in the calculated profiles. As a consequence, the 5%/0.3 mm gamma-pass-rates were only 80%–90% for the in-air profiles for four wheel covering ranges from 10 to 35 mm (see Table A1).

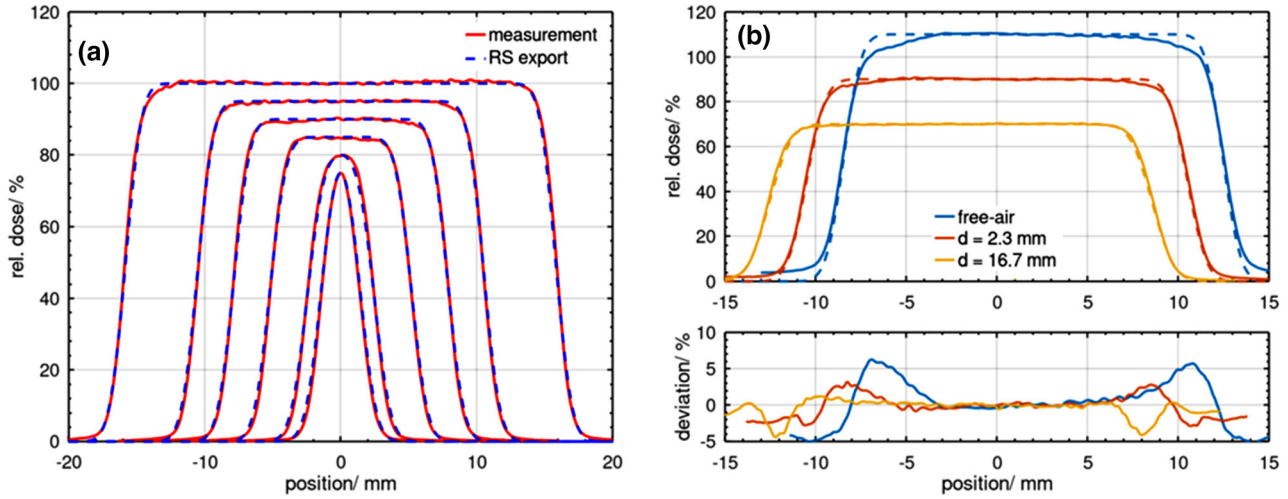

FIGURE 6 (a) Comparison of mid-SOBP (spread-out Bragg peak) cross-profiles for circular aperture openings with diameters from 5 to 30 mm (*R25M20*). (b) Comparison of lateral profiles of a 20 × 20 mm^2 mm field in various depths of *R25M20* where the corresponding difference plot is shown in the lower graph. (Profiles are normalized to respective center and scaled/shifted for better visibility.)

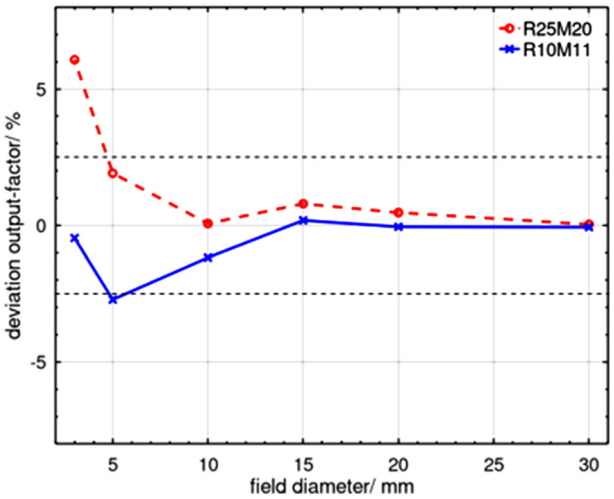

FIGURE 7 Deviation of output-factor between calculation and measurement. The output-factor is given for circular shaped fields of various diameters, normalized to the measurement in a 20 mm × 20 mm field. Output-factors were obtained at mid-SOBP (spread-out Bragg peak) for *R25M20* (red markers, dashed line) and *R10M11* (blue markers, solid line). Single-measurement points are connected to guide the eyes. The dashed horizontal line indicates a ±2.5% deviation.

3.2.2 | Output-factor modeling

Figure 7 shows the deviation of calculated, relative output-factors in two wheel/stop-block combinations for field-sizes down to 3 mm diameter. Measurements were based on the microSilicon detector, normalized to a 20 mm × 20 mm field. The agreement between calculation and measurement in terms of the output-factor is within ±2.5% down to a 5 mm diameter. As no aperture-scatter is modeled in RayOcular, the output-factor is only influenced by the lateral scatter in medium and the lateral extent of the fluence distribution for underlying pencil beams.

3.2.3 | Modeling the impact of wedges

Figure 8 shows some examples of measured and computed lateral profiles for fields using wedges. The effect of the wedge is clearly seen as a broadening of the lateral penumbra at the thick wedge side of the profile, a characteristic bump in the dose plateau at a position related to the thin edge of the wedge, and a narrowing of the field due to the pull back of the dose. In general, Figure 8 shows that the calculations predict these effects well.

Table 2 summarizes the results for lateral profiles and depth–dose curves. The results for lateral profiles were analyzed at two depths: $d = R - 1/3M$ and $d = R - 2/3M$. The larger depth shows pass-rates in the gamma-test of >90% with 2%/0.3 mm and 100% with 3%/0.5 mm. The gamma-pass-rates for the profiles at shallower depths are clearly not as good, especially for 2%/0.3 mm. The reduction in range caused by the wedges is systematically overestimated by up to 0.6 mm, which somehow seems to be correlated with a corresponding increase in DFO (90%–10%) of up to 0.6 mm.

4 | DISCUSSION

4.1 | Geometric modeling and image handling

The deviations between modeled and visible clip positions in the X-ray images were observed to be within 0.3 mm.

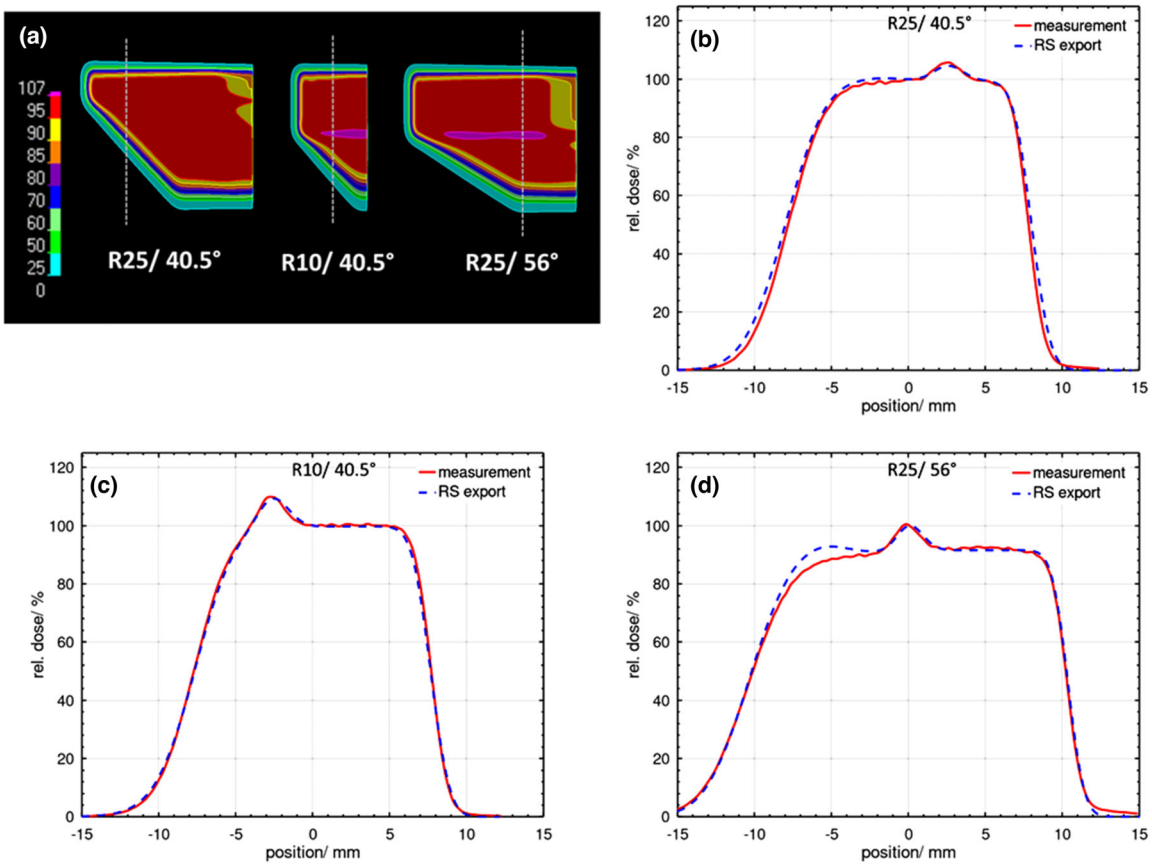

FIGURE 8 Examples for the comparison of measured and calculated cross-profiles in a beam with wedge. (a) Illustration of relative dose distributions in percent as modified by a wedge for selected setups in Table 2 (marked by an asterisk). (b–d) Measured and calculated lateral cross-profiles of the three configurations in (a). All profiles are normalized to the field center. The depth was $d = R - M/3$ for (b and c) and $d = R - 2/3M$ for (d).

The deviations can be attributed to uncertainties in the localization of model clips in the CT images, which in the case of the Tantalum clips are strongly affected by defining the clip center in the CT-artifacts. In the investigated phantom, the deviations between measured and modeled clip-to-clip distances were up to 0.3 mm. Although titanium was shown by Daftari et al.[24] to be a reasonably alternative, to the authors' knowledge, only clips from Tantalum are commercially available.

There are other conceivable sources for error here. The matching between clip models and X-ray images in RayOcular is accomplished by manually altering the apparent eye center position and fixation light angles. This process is to some degree user-dependent, but the RayOcular system currently does not support an automatic matching such as offered in EYEPLAN.[3] Further, the clip models in the 3D eye model are created as tangential to the sclera structure. Due to the suturing process, the clips may not be perfectly perpendicular, and in the case of the used phantom (Figure 1a), the clips were not necessarily glued perfectly to the ball itself. As a result, small deviations in its shape may have influenced the judgment of the best match. Hence, the overall agreement of ∼0.3 mm considers more than just modeling in RayOcular and needs to be put in perspective of the clinical requirements in OPT. Given the current margin concepts, a 0.5 mm setup uncertainty is deemed appropriate[12,16] and thus the determined agreement in this study is considered acceptable.

The 3D-printed phantom (Figure 1b) was designed for realizing well-defined, discrete orientations of the eye. Despite this, the matching included corrections of up to 3° in the three angles. This can be attributed to the manual placement of the phantom and some imperfections in its construction. The judged agreement is further affected by the imaging geometry in terms of SAD, SID, and detector size. The parameters were provided by the vendor (IBA) and are part of the beam-model. Inaccuracies in the measurement can translate to mismatch of the model projections.

The registration of funduscopic images to a fundus view is an important feature when the tumor volume is defined in the fundus view. This process is rather complex due to the complex relation between the funduscopic image and the 3D model and by the fact that there are few landmarks in the eye that can verify a successful registration. Despite this, a quantitative evaluation of the accuracy of this registration by means of

TABLE 2 Summary of comparison between calculation and measurement for different setups with wedges for lateral and depth–dose scans

Lateral profiles						
Angle/°	**Range/mm**	**Offset/mm**	**Depth**	**2%/0.3 mm**	**3%/0.5 mm**	**ΔLP/mm**
26.3	25	0	$R - 2/3M$	92.0	100	−0.2
26.3	25	0	$R - 1/3M$	99.2	100	0.0
40.5	25	0	$R - 2/3M$	89.0	96.9	−0.4
40.5	25	0	$R - 1/3M$	97.6	100	−0.1
40.5	25	0.5	$R - 2/3M$	93.6	100	−0.2
40.5	25	0.5	$R - 1/3M$	100	100	0.0
40.5	25	−0.5	$R - 2/3M$	78.5	90.4	−0.4
40.5	**25**	**−0.5**	$\boldsymbol{R - 1/3M}$	**92.7**	**100**	**0.2**
40.5	**10**	**0**	$\boldsymbol{R - 2/3M}$	**100**	**100**	**0.1**
40.5	10	0	$R - 1/3M$	100	100	0.2
40.5	35	0	$R - 2/3M$	92.5	100	−0.2
40.5	35	0	$R - 1/3M$	91.5	100	0.0
56	**25**	**0**	$\boldsymbol{R - 2/3M}$	**81.6**	**87.7**	**−0.4**
56	25	0	$R - 1/3M$	100	100	0.2

Depth profiles					
Angle/°	**Range/mm**	**Offset/mm**	**2%/0.3 mm**	**ΔDFO/mm**	**Δ*R*90/mm**
26.3	25	−0.5	100	0.2	−0.1
40.5	25	−0.5	95.5	0.5	−0.4
40.5	10	−0.5	100	0.3	−0.1
56	25	−0.5	77.6	0.6	−0.6

Note: The results of a 1D-gamma-test as well as the difference in the lateral penumbra (80%–20%) (LP) is given for two depths, that is, $d = R - 2/3M$ and $d = R - M/3$. LP is only analyzed for the part of the profile affected by the thick end of the wedge. The results for the DD-scans provide the difference DFO and range (R90). The results for the 3%/0.5 mm test are omitted for the DD scans as passing rate was always 100%. The offset describes the position of the thin edge of the wedge with respect to the center of a 20 mm × 20 mm field, that is, a negative sign indicates the wedge covering the field center. The values in bold indicate the setups shown in Figure 8b–d.

Abbreviation: DFO, distal falloff.

a phantom has, at least to the authors' knowledge, not been previously reported for any TPS. In this work, we could show that RayOcular could reproduce the known landmark distances in the fundus view within ∼0.8 mm. The accuracy of the overlay is affected by the quality of the funduscopic image, which depends on the camera used, and the quantitative analysis is further limited by the resolution of displayed distances in RayStation with 0.1 mm.

The design of the 3D-printed phantom aimed at a realistic representation of a human eye, but it needs to be emphasized that it has limitations. For instance, the refraction index of a real human eye is slightly lower, but age dependent and even variable throughout the lens itself.[20] Further, the model does not consider the cornea/anterior chamber that has a refractive effect. To this point, the impact on acquired fundus images is not exactly known. Given the general variability of the human eye, the phantom is considered an appropriate representation.

In this study, using RayOcular, there was no difference in measured distances between the view in polar or camera mode. Daftari et al., on the other hand, estimated the effect of changing between a Cartesian and spherical coordinates with up 2.5 mm.[4] The camera mode may seem to represent image formation process more appropriately; however, in RayStation, it is associated with several free optical parameters, which are normally not available from the manufacturer of the fundus photo camera. The camera mode may also not be appropriate when the funduscopic image is composed of several images that have been patched together.

The quality of the tumor definition in a fundus view is strongly impacted by the registration, especially the scaling. This registration depends on the optic disc to macula distance that can accurately be determined in OCT, but also on the relative angle between those two structures that cannot be determined by any measurements. The overall deviation even for the well-registered phantom image with <1 mm here is typically considered in corresponding margins during the contouring process.

The phantom used in this study was designed to be cylindrically symmetric around the central axis of the eye. However, the deviation between modeled and measured distances in the eye shown in Figure 4 varied among directions from distal pole in which the deviations were determined. This points toward imperfections in experimental setup, more precisely the alignment of

the lens and/or the phantom itself when the funduscopic image was acquired. On the other hand, the setup and alignment of a clinical funduscopic image of a human eye are also not expected to be perfect in these respects, meaning that the deviation observed in Figure 4 could very well reflect a clinical situation and give a hint of the associated uncertainties. It is envisioned to extend the phantom study to more cases and different designs for a better understanding of limitations in the imaging and registration process of funduscopy. More research is required to fully exploit the limitations in the funduscopy registration and the concept of the 3D-printed eye-phantom is considered a reasonable approach.

4.2 | Dosimetric evaluation

The agreement between computed and measured doses was in general very good and well within the defined tolerances. This was true for depth–doses and lateral profiles of open fields but with some degradation for fields that employ a wedge. The exception concerned the in-air and shallow lateral profiles (Figure 6b). Here, a kind of dome-shape in the measured profiles was not accurately reproduced in the computed profiles, leading to a lower passing rate and even affecting the lateral penumbra width. This effect can be explained by the design of the IBA single scattering nozzle, as described by Slopsema et al.[16] Preliminary Monte Carlo calculations show that protons are scattered in the range-verifier system in the nozzle, which leads to the creation of lower energy protons with mean energy of 20 MeV, which are unevenly laterally distributed over the treatment field. This cannot be reproduced in the dose calculation as RayOcular assumes a laterally flat field upstream of the aperture and considers the angular confusion to be depth-independent. In this context, we point out that the measured and calculated profiles shown in Figure 6 are normalized at the center point of each profile. In terms of absolute dose, it appears more likely that the measured profiles would exhibit a relatively higher dose at the center, whereas the computed and measured profiles would match better around the profile shoulders.

In Figure 8d, a discrepancy between calculated and measured dose in the left part of the high dose region can be seen. The underlying reason for this discrepancy is currently not known, although it seems reasonable to think that it is related to the same effect that led to the dome-shaped profiles seen in Figure 6b. The dose discrepancy disappeared at greater depths ($=R - M/3$) for the same field (not shown). The slightly worse agreements between calculation and measurement for the setups with wedges need to be put in perspective. Besides the previously mentioned limitation in reproducing the initial scatter, the depth–dose measurement in the laterally varying dose distribution is strongly affected by position uncertainties. For instance, the 56° wedge creates a gradient with a roughly 1:2 relationship between lateral position and distal range, that is, an offset of 0.1 mm in lateral position translates to a change of 0.2 mm in distal range. It is also worth noting that the wedge-induced excess dose and significant broadening of lateral penumbra seen in this study are completely ignored in the dose calculation algorithms of the other currently used OPT TPSs.

The agreement in the output-factor is considered sufficient with ±1% at 10 mm field diameter and ±2.5% at 5 mm. Clinically, a target diameter <5 mm can be considered impossible as long as a 2.5 mm lateral margin is used. The deviations further need to be viewed in the context of the measurement uncertainty for such small fields with sharp gradients where a slight positioning uncertainty has a correspondingly high influence on the measured signal.[25] It should also be remembered that RayStation does not provide absolute output for passive fields, which means that the observed correctness of the RayStation "output-factor" should be viewed as a convenience, or as a secondary output check in the external determination of field-specific MUs.

5 | CONCLUSION

The RayOcular module was validated for clinical use with the IBA OPT dedicated fixed beam delivery system of the West German Proton Therapy Centre in Essen, Germany.

The accuracy of the clip positions in the RayOcular 3D model as determined from CT scans of eye-phantoms was found to be satisfactory when comparing projections of the clip models to the visible clips of the phantoms in imported orthogonal X-ray images. The agreement between modeled and imaged clips was ~0.3 mm.

A funduscopic image of a 3D-printed eye-phantom, including a realistic lens, was registered in the RayOcular fundus view, and Euclidian distances between landmarks seen in the photo were measured in the fundus view. The fundus view measured distances were found to be within 1 mm from the known values, where the largest discrepancies were found in the most anterior landmarks (60° polar angle from the posterior pole). Results depend on registration accuracy that, in a clinical setting, is mainly affected by the physiological distance between macula and optic disc.

A grand majority of the calculated depth–dose curves and lateral profiles at various ranges, modulations, aperture openings depths, including the use of wedges, exhibits a gamma-pass-rate (2%/0.3 mm) greater than 90% when compared to measurements. Furthermore, the calculated range of the lateral as well as the distal penumbra widths is within 0.2 mm to the measured ones for most investigated cases. However, the impact of

scatter in the range verifier in the IBA nozzle is not modeled in the TPS, and thus for shallower depths the discrepancy between measurement and calculation increases due to the resulting non-flat profiles.

The impact of wedges is represented by the pencil-beam-based dose algorithm of RayOcular. The wedge-induced penumbra broadening, reduction in range, and the excess dose seen in the measurements are accurately reproduced in the calculations. This is a major improvement compared to the currently used OPT TPSs where the excess scattering of the beam in the wedge is not explicitly considered leading to a significant underestimation of the lateral penumbra on the thick wedge side of the field. As wedges are often used to spare optic disc and/or macula, an accurate calculation of applied dose to those organs-at-risk is obviously important for individual treatment planning as well as investigation of outcome for a large cohort of patients.

ACKNOWLEDGMENTS

Tim Ormeloh is acknowledged for designing phantoms and Felix Junkers, Manuel Beck, and Osamah Ghanem (WPE) for their support in experimental measurements. Jorn Verwey (TreesWithCharacter) is acknowledged for sharing his experience in ocular proton therapy. Stiftung UME is acknowledged for the acquisition of the 3D-printer used for the construction of the phantoms, which in turn was carried out by Manuel Beck and Julian Kinne. The authors thank Erik Vidholm (RaySearch) for discussions on the hierarchical eye model in RayStation.

CONFLICT OF INTEREST

Martin Janson is an employee of RaySearch Laboratories (Stockholm, Sweden), the company that has developed and is selling the treatment planning system RayStation. The other authors do not have any conflict of interest.

REFERENCES

1. Goitein M, Miller T. Planning proton therapy of the eye. *Med Phys*. 1983;10(3):275-283.
2. Hrbacek J, Mishra KK, Kacperek A, et al. Practice patterns analysis of ocular proton therapy centers: the international OPTIC survey. *Int J Radiat Oncol Biol Phys*. 2016;95(1):336-343.
3. Kacperek A. Ocular proton therapy centers. In: Linz U, ed. *Ion Beam Therapy – Fundamentals, Technology, Clinical Applications*. Springer-Verlag; 2012:149-177.
4. Daftari IK, Mishra KK, O'Brien JM, et al. Fundus image fusion in EYEPLAN software: an evaluation of a novel technique for ocular melanoma radiation treatment planning. *Med Phys*. 2010;37(10):5199-5207.
5. Sas-Korczyńska B, Markiewicz A, Romanowska-Dixon B, Pluta F. Preliminary results of proton radiotherapy for choroidal melanoma – the Kraków experience. *Contemp Oncol (Pozn)*. 2014;18(5):359-366.
6. Titt U, Suzuki K, Li Y, Sahoo N, Gillin MT, Zhu XR. Technical note: Dosimetric characteristics of the ocular beam line and commissioning data for an ocular proton therapy planning system at the Proton Therapy Center Houston. *Med Phys*. 2017;44(12):6661-6671.
7. Saini J, Maes D, Egan A, et al. Dosimetric evaluation of a commercial proton spot scanning Monte-Carlo dose algorithm: comparisons against measurements and simulations. *Phys Med Biol*. 2017;62(19):7659-7681.
8. Pfeiffer K, Dobler B, Rethfeldt C, Schlegel W, Bend R. OCTOPUS, a planning tool for proton therapy of eye tumours. In: *The Use of Computers in Radiation Therapy*. Springer Berlin Heidelberg; 2000.
9. Dobler B, Bendl R. Precise modelling of the eye for proton therapy of intra-ocular tumours. *Phys Med Biol*. 2002;47(4):593-613.
10. Denker A, Cordini D, Heufelder J, et al. Ion accelerator applications in medicine and cultural heritage. *Nucl Instrum Methods Phys Res A*. 2007;580(1):457-461.
11. Fleury E, Trnková P, Erdal E, et al. Three-dimensional MRI-based treatment planning approach for non-invasive ocular proton therapy. *Med Phys*. 2021;48(3):1315-1326.
12. Wulff J, Koska B, Janson M, et al. Technical note: Impact of beam properties for uveal melanoma proton therapy—an in silico planning study. *Med Phys*. 2022;49:3481-3488.
13. Rethfeldt C, Fuchs H, Gardey KU. Dose distributions of a proton beam for eye tumor therapy: hybrid pencil-beam ray-tracing calculations. *Med Phys*. 2006;33(3):782-791.
14. Baker C, Kacperek A. The influence of physical wedges on penumbra and in-field dose uniformity in ocular proton beams. *Physica Med*. 2016;32(4):612-617.
15. Marnitz S, Cordini D, Bendl R, et al. Proton therapy of uveal melanomas: intercomparison of MRI-based and conventional treatment planning. *Strahlenther Onkol*. 2006;182(7):395-399.
16. Slopsema RL, Mamalui M, Zhao T, Yeung D, Malyapa R, Li Z. Dosimetric properties of a proton beamline dedicated to the treatment of ocular disease. *Med Phys*. 2014;41(1):011707.
17. RaySearchLaboratories. RSL-D-RS-10B-REF, RayStation 10B Reference Manual. 2020.
18. Soukup M, Fippel M, Alber M. A pencil beam algorithm for intensity modulated proton therapy derived from Monte Carlo simulations. *Phys Med Biol*. 2005;50(21):5089-5104.
19. Deasy JO. A proton dose calculation algorithm for conformal therapy simulations based on Molière's theory of lateral deflections. *Med Phys*. 1998;25(4):476-483.
20. Atchison DA, Thibos LN. Optical models of the human eye. *Clin Exp Optom*. 2016;99(2):99-106.
21. Eaton JW, Bateman D, Hauberg S, Wehbring R. *GNU Octave Version 5.2.0 Manual: A High-Level Interactive Language for Numerical Computations*. 2020.
22. Geurts M. *1D, 2D, or 3D Gamma Computation in MATLAB*. 2015. https://github.com/mwgeurts/gamma
23. Ma CMC, Chetty IJ, Deng J, et al. Beam modeling and beam model commissioning for Monte Carlo dose calculation-based radiation therapy treatment planning: report of AAPM Task Group 157. *Med Phys*. 2020;47(1):e1-e18.
24. Daftari IK, Quivey JM, Chang JS, Mishra KK. Technical note: Feasibility study of titanium markers in choroidal melanoma localization for proton beam radiation therapy. *Med Phys*. 2018;45(3):1036-1039.
25. Palmans H, Andreo P, Huq MS, Seuntjens J, Christaki KE, Meghzifene A. Dosimetry of small static fields used in external photon beam radiotherapy: summary of TRS-483, the IAEA-AAPM international Code of Practice for reference and relative dose determination. *Med Phys*. 2018;45(11):e1123-e1145.

How to cite this article: Wulff J, Koska B, Heufelder J, et al. Commissioning and validation of a novel commercial TPS for ocular proton therapy. *Med. Phys.*. 2022;1-15. https://doi.org/10.1002/mp.16006

APPENDIX

TABLE A1 Comparison between measurements and calculation for lateral profiles in different setups

Isocenter at middle of SOBP/measurement depth = middle of SOBP							
Range/modulation	**Aperture (mm^2)**	**1%/0.3 mm**		**2%/0.3 mm**		**ΔLP/mm**	
*R*35*M*19.8	10 × 10	100.0	100.0	100.0	100.0	≤0.1	≤0.1
	20 × 20	90.0	90.8	100.0	99.6	≤0.1	≤0.1
*R*32*M*19.8	10 × 10	100.0	100.0	100.0	100.0	≤0.1	≤0.1
	20 × 20	90.3	91.9	98.3	100.0	≤0.1	≤0.1
*R*27*M*19.9	10 × 10	100.0	100.0	100.0	100.0	≤0.1	≤0.1
	20 × 20	92.4	91.9	100.0	99.6	≤0.1	≤0.1
*R*24*M*20.56	10 × 10	100.0	100.0	100.0	100.0	≤0.1	≤0.1
	20 × 20	90.7	93.6	95.8	100.0	≤0.1	≤0.1
*R*19*M*20	10 × 10	100.0	100.0	100.0	100.0	≤0.1	≤0.1
	20 × 20	92.4	95.3	98.3	100.0	≤0.1	≤0.1
*R*15*M*16	10 × 10	100.0	100.0	100.0	100.0	≤0.1	≤0.1
	20 × 20	93.7	94.1	98.7	100.0	≤0.1	≤0.1
*R*10*M*11	10 × 10	100.0	100.0	100.0	100.0	≤0.1	≤0.1
	20 × 20	91.2	94.5	99.2	100.0	≤0.1	≤0.1
Isocenter at phantom surface/measurement depth = middle of SOBP							
Range/modulation	**Aperture**	**1%/0.3 mm**		**2%/0.3 mm**		**ΔLP/mm**	
*R*25*M*20	*d* = 30 mm	97.4	94.8	100.0	100.0	0.1	0.1
	d = 20 mm	97.5	90.3	100.0	99.6	0.1	0.1
	d = 15 mm	95.7	87.0	100.0	98.9	0.1	0.1
	d = 10 mm	100	100.0	100.0	100.0	0.2	0.1
	d = 5 mm	100	100.0	100.0	100.0	0.2	0.1
	d = 3 mm	100	100.0	100.0	100.0	0.1	0.1
	20 × 20 mm^2	91.3	95.9	100.0	100.0	0.1	0.2
Measurement free-air at isocenter							
Range/modulation	**Aperture**	**3%/0.3 mm**		**5%/0.3 mm**		**ΔLP/mm**	
*R*35*M*35	20 × 20 mm^2	66.2	66.9	79.3	78.2	−0.2	−0.2
*R*24*M*25		71.6	70.6	86.0	84.7	−0.3	−0.2
*R*19*M*20		69.9	72.1	84.8	85.8	−0.3	−0.3
*R*10*M*11		74.5	74.4	89.4	91.7	−0.4	−0.3

Note: The results of a 1D-gamma-test is shown in the *x*- and *y*-direction. The difference in the lateral penumbra (80%–20%) (LP) is given as maximum of both directions.
Abbreviation: SOBP, spread-out Bragg peak.